ACS OMEGA

http://pubs.acs.org/journal/acsodf

Article

New Polymorphic Modifications of 6-Methyluracil: An Experimental and Quantum Chemical Study

Svitlana V. Shishkina,* Anna M. Shaposhnik, Victoriya V. Dyakonenko, Vyacheslav M. Baumer, Vitalii V. Rudiuk, Igor B. Yanchuk, and Igor A. Levandovskiy

Cite This: *ACS Omega* 2023, 8, 20661−20674

Read Online

ACCESS | Metrics & More | Article Recommendations | Supporting Information

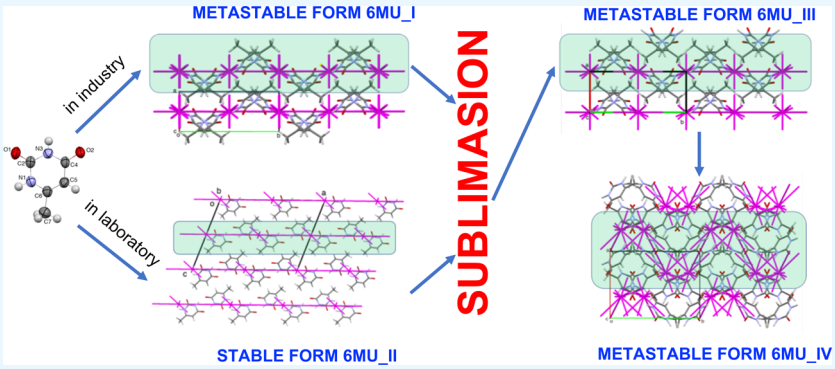

ABSTRACT: Polymorphism of 6-methyluracil, which affects the regulation of lipid peroxidation and wound healing, has been studied by experimental and quantum chemical methods. Two known polymorphic modifications and two new crystalline forms were crystallized and characterized by single crystal and powder X-ray diffraction (XRD) methods as well as by the differential scanning calorimetry (DSC) method and infrared (IR) spectroscopy. The calculations of pairwise interaction energies between molecules and lattice energies in periodic boundary conditions have shown that the polymorphic form **6MU_I** used in the pharmaceutical industry and two new forms **6MU_III** and **6MU_IV**, which can be formed due to temperature violations, may be considered as metastable. The centrosymmetric dimer bound by two N−H···O hydrogen bonds was recognized as a dimeric building unit in all of the polymorphic forms of 6-methyluracil. Four polymorphic forms have a layered structure from the viewpoint of interaction energies between dimeric building units. The layers parallel to the (100) crystallographic plane were recognized as a basic structural motif in the **6MU_I**, **6MU_III**, and **6MU_IV** crystals. In the **6MU_II** structure, a basic structural motif is a layer parallel to the (001) crystallographic plane. The ratio between the interaction energies within the basic structural motif and between neighboring layers correlates with the relative stability of the studied polymorphic forms. The most stable polymorphic form **6MU_II** has the most anisotropic "energetic" structure, while the interaction energies in the least stable form **6MU_IV** are very close in various directions. The modeling of shear deformations of layers in the metastable polymorphic structures has not revealed any possibility of these crystals to be deformed under external mechanical stress or pressure influence. These results allow the use of metastable polymorphic forms of 6-methyluracil in the pharmaceutical industry without any limitations.

INTRODUCTION

The polymorphism study of biologically active molecules pursues both theoretical and practical aims.[1−3] The conditions for the formation of various crystal structures are of great theoretical interest, and this knowledge leads to the development of crystal engineering principles. Different physicochemical and biological properties (bioavailability, dissolution rate) of polymorphic forms are of great importance to the pharmaceutical industry.[4,5] Crystallization of a new polymorph of an active pharmaceutical ingredient (API) can result in a change of manufacturability, stability, reproducibility, and biological activity of the drug.[6−8] This process is difficult to control, and the formation of a new crystal form can be caused by minimal changes in a solution concentration, crystallization rate, temperature, grinding conditions, or tableting pressure. Unfortunately, the appearance of a new polymorphic form can be a reason for significant financial losses for a pharmaceutical company, as happened with the manufacturers of Tegretol, Norvir, Vermox, Coumadin, or Neupro.[3,9,10] So, finding all of the ways to obtain as many polymorphic forms of a drug as

Received: February 23, 2023
Accepted: May 22, 2023
Published: May 31, 2023

Table 1. Crystallographic Data for 6MU Polymorphic Forms

polymorph	6MU_I	6MU_II	6MU_III	6MU_IV
empirical formula	$C_5H_6N_2O_2$			
formula weight, a.m.u.	126.12			
crystal system	monoclinic			
space group	*P*21/*c*	*C*2/*c*	*P*21/*c*	*P*21/*c*
a (Å)	4.5194(14)	20.537(3)	4.6081(7)	9.3874(15)
b (Å)	10.9811(18)	3.9108(4)	10.767(3)	11.6695(13)
c (Å)	11.7294(14)	14.801(3)	11.881(4)	11.3883(17)
β°	97.750(16)	110.972(19)	99.76(2)	112.516(18)
V (Å^3)	576.8(2)	1110.0(3)	580.9(3)	1152.4(3)
Z	4	8	4	8
ρ (g·cm^{-3})	1.452	1.509	1.442	1.454
μ (mm^{-1})	0.115	0.119	0.114	0.115
F(000)	264	528	264	528
reflections collected/unique	3320/1016	4163/979	3513/1023	4252/2019
R_{int}	0.0974	0.1314	0.1403	0.0518
parameters	92	92	92	185
final R_1 values ($I > 2\sigma(I)$)	0.0711	0.0871	0.0816	0.0782
final w$R_2(F^2)$ values ($I > 2\sigma(I)$)	0.1771	0.2031	0.1945	0.2355
goodness-of-fit on F^2	0.998	1.027	0.961	1.076
CCDC	2243617	2243620	2243618	2243619

possible and study them thoroughly is a very important task for crystallographers and pharmaceutical chemists.

Being one of four nucleobases in a nucleic acid, uracil was found in RNA while its derivative 5-methyluracil or thymine was found in DNA. These compounds are well known for more than a century but their polymorphism is poorly studied. There are no polymorphic modifications of uracil in the Cambridge Crystal Structure Database[11] while polymorphic modifications of 5-methyluracil were found and thoroughly studied only recently.[12,13] 6-Methyluracil is the closest analogue of uracil and 5-methyluracil but it can be obtained only synthetically.[14,15] This compound is widely used in pharmaceutics as a drug affecting the regulation of lipid peroxidation and healing of wounds.[16,17] 6-Methyluracil is also used as a component of complex compositions. For example, the complex with *N*-methyl-D-glucamine was proposed for the treatment of a variety of medical conditions characterized by excessive or inappropriate apoptosis such as ischemia, type I diabetes, stroke, and Alzheimer's and Parkinson's diseases.[18,19]

First, the molecular and crystal structure of 6-methyluracil was determined by the powder diffraction study.[20] The accuracy of this method did not allow us to determine the positions of hydrogen atoms. A more preferable diketo tautomeric form of this very simple conformationally rigid molecule has been proposed based on the bond lengths, which have also been determined with high inaccuracy. The keto−enol tautomerism of 6-methyluracil was studied by the gas-phase electron diffraction and quantum chemical methods.[21,22] The diketo form of 6-methyluracil was confirmed by further X-ray diffraction (XRD) studies that revealed the second polymorphic form of this compound.[23,24] It should be noted that polymorph **II** was crystallized from water[23] or from DMF[24] while polymorph **I** was named pharmaceutical and any reliable information about its crystallization is absent. In addition, Leonidov and co-workers discussed a possible difference in the biological activity of two polymorphic forms of 6-methyluracil based on the difference in their crystal packing.[25] However, this discussion has not been confirmed by experimental data.

Thus, we can conclude that the polymorphism of 6-methyluracil has not been investigated systematically. In the present study, we have re-determined 6-methyluracil polymorphic form **I** and found new polymorphic forms of this pharmaceutically important compound.

RESULTS AND DISCUSSION

Search for Polymorphic Forms of 6MU. Being a very effective drug, **6MU** is manufactured by the pharmaceutical industry in the tablet form or as an ointment. Therefore, the control of its polymorphic form is of great importance for the quality of the final product. The analysis of the pharmaceutical substance (API) has revealed that **6MU** exists rather in polymorphic form **I** (**6MU_I**) that has been determined only by powder diffraction data which have low enough quality.[20] So these data proved to be not very good for a reliable analysis of API and need to be improved.

Our attempts to crystallize **6MU** from various solvents have always led to the formation of needle-like crystals of the polymorphic form **II**. Even crystallization from water used in the technological process did not give the polymorph **6MU_I** in the laboratory. The main difference between crystallization in the technological process and in the laboratory is not the solvent used, but the volume of the crystallizing mixture and the stirring of the solution during the crystallization process. Thus, it can be presumed that the gradient of temperature decrease and the inertness of the reaction mixture can play a key role in the formation of the polymorph **6MU_I** during the technological process.

To exclude the solvation effects, an attempt was made to crystallize **6MU** from the melt. A sample of polymorph **6MU_I** was dissolved in water, boiled, and dried. Then the obtained powder was heated up to the sintering temperature (heating up to the melting point was not performed to avoid compound decomposition). The analysis of the obtained sample by powder diffraction has revealed that the main crystal phase is the polymorph **6MU_II** but an impurity of a new phase can be found. Indeed, a more thorough analysis has revealed needle-like crystals of a new polymorph **6MU_III** and prism-like

https://doi.org/10.1021/acsomega.3c01231
ACS Omega 2023, 8, 20661−20674

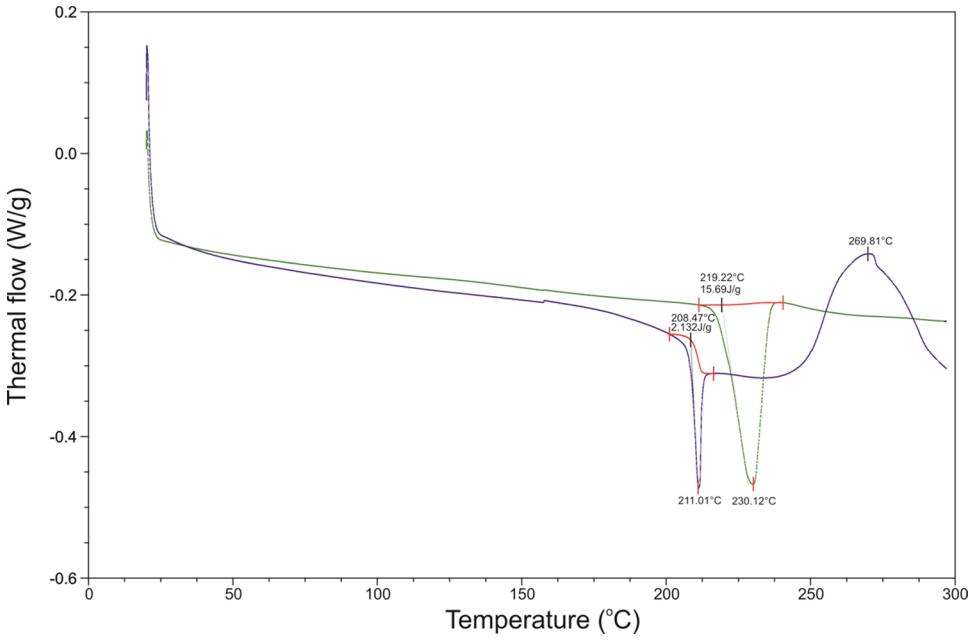

Figure 1. DSC thermograms of polymorph **6MU_I** (at the top) and **6MU_II** (at the bottom).

Table 2. Powder Diffraction Data of the 6MU Sample at Different Temperatures According to Rietveld Refinement

T, °C	Phase	*a*, Å	*b*, Å	*c*, Å	*β*, deg	*V*, Å^3
RT	**6MU_I**	4.4983(1)	11.0352(5)	11.7277(4)	97.283(4)	577.46(4)
100	**6MU_I**	4.4948(1)	11.0374(6)	11.7197(4)	97.215(4)	576.81(4)
140	**6MU_I**	4.4967(1)	11.0360(6)	11.7212(4)	97.246(4)	577.02(4)
180	**6MU_I**	4.5120(1)	11.0059(5)	11.7331(4)	97.503(4)	577.66(4)
200	**6MU_III**	4.5406(1)	10.9419(6)	11.7647(4)	98.094(4)	578.67(4)
210	**6MU_III**	4.5610(1)	10.9025(6)	11.7851(4)	98.500(4)	579.58(4)
	6MU_II 3%[a]	20.5131(1)	3.9147(5)	14.8193(2)	111.022(3)	1110.82(3)
245	**6MU_III**	4.5866(2)	10.8437(8)	11.8212(5)	99.086(6)	580.57(6)
	6MU_IV 11%[a]	9.416(5)	11.731(9)	11.325(2)	112.14(2)	1158.6(1)
	6MU_II 12%[a]	20.732(1)	3.9227(8)	14.831(2)	111.22(2)	1124.4(7)
275	**6MU_IV**	9.3925(4)	11.6622(5)	11.3664(5)	112.392(2)	1151.17(8)
290	**6MU_IV**	9.3944(3)	11.6577(4)	11.3654(4)	112.420(1)	1150.61(6)

[a]The phase ratio was calculated using the Rietveld method.

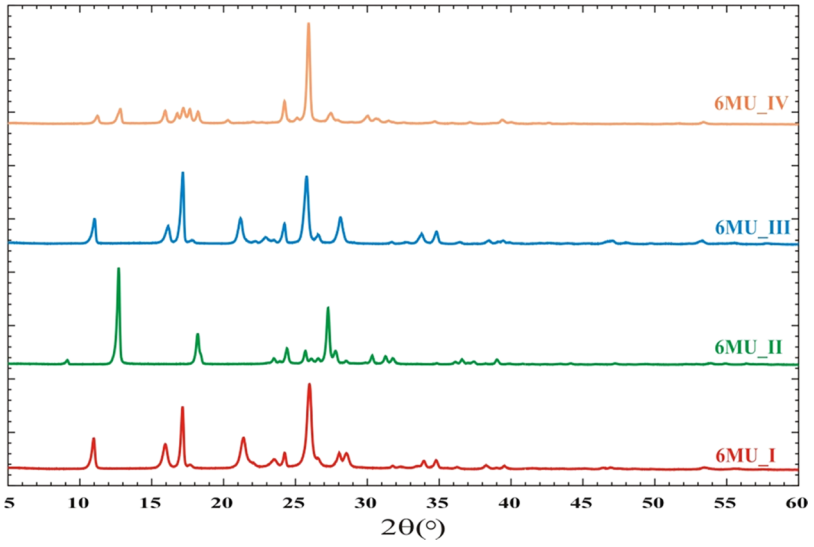

Figure 2. Powder X-ray diffraction patterns of **6MU** polymorphic forms.

https://doi.org/10.1021/acsomega.3c01231
ACS Omega 2023, 8, 20661−20674

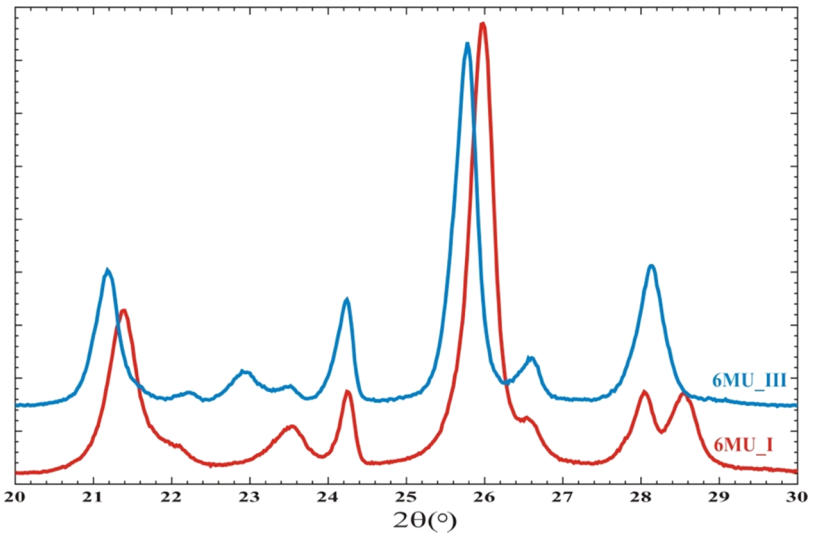

Figure 3. Powder X-ray diffraction patterns of **6MU_I** and **6MU_III** in the 2Θ region from 20 to 30°.

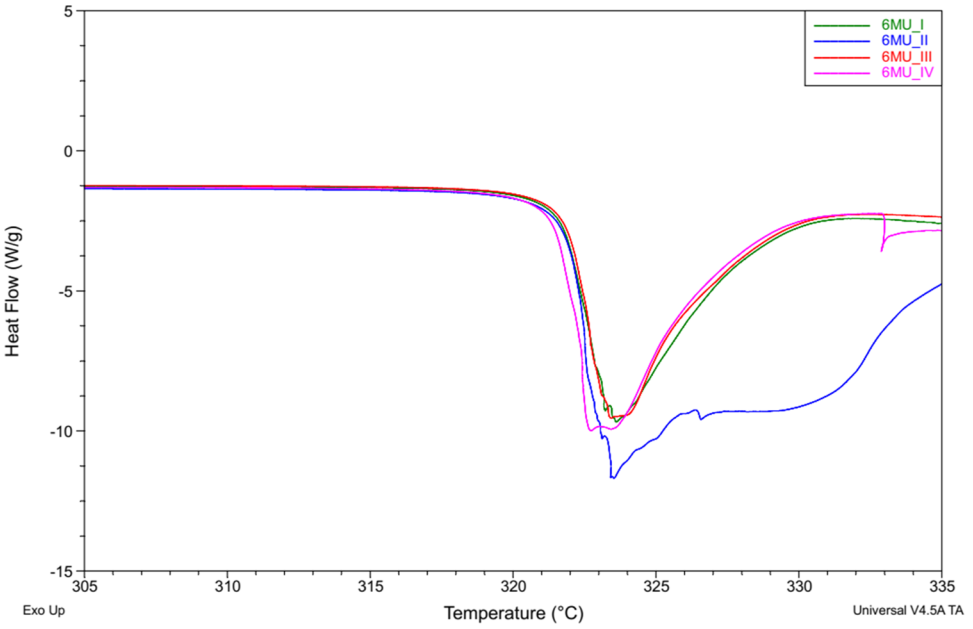

Figure 4. DSC curves measured for pure samples of **6MU_I**, **6MU_II**, **6MU_III**, and **6MU_IV**.

crystals of a new polymorph **6MU_IV** in the pre-melting sample. Both new polymorphs of **6MU** were identified primarily by the single crystal X-ray analysis (Table 1). It should be noted that unit cell parameters of form **6MU_III** are very close to the ones determined for polymorph **6MU_I**. Therefore, additional arguments are needed to prove the existence of form **6MU_III** as a new polymorph.

To separate new polymorphic forms **6MU_III** and **6MU_IV** as a pure crystal phase, DSC thermograms of the polymorphs **6MU_I** and **6MU_II** (Figure 1) have been studied thoroughly. Polymorphic crystals **6MU_I** have been heated in a double Petri dish up to a temperature below the endothermic effect found in the DSC thermogram (Figure 1, at the top). It was found that partial sublimation of the sample (white haze can be seen) occurs at ∼200 °C, and the product was crystallized on the cover dish as very thin needles of polymorph **6MU_III**. Heating up to a temperature of 250 °C led to re-crystallizing of the powder mass in the bottom dish giving elongated prismatic crystals of the polymorph **6MU_IV**. It should be noted that crystals of **6MU_IV** obtained at this temperature contained crystals of **6MU_III** as an impurity and were purified due to further heating up to ∼270 °C.

The additional study of the **6MU_I** heating process was performed by the powder diffraction method. A sample of polymorph **6MU_I** was heated up to various temperatures and analyzed using the Rietveld method (Table 2). The data obtained have confirmed the formation of polymorph **6MU_III** at 200 °C and polymorph **6MU_IV** at 245 °C and above. In addition, the presence of the polymorphic form **6MU_II** as an impurity within the temperature range of 210−245 °C may explain some of the problems with an ointment containing **6MU** due to the appearance of grains.

The same study was carried out for the polymorphic form **6MU_II**. Being more stable than the polymorph **6MU_I**, these crystals sublimated at 230 °C. As a result, coarse crystals of **6MU_IV** were formed without any impurity of the polymorph

https://doi.org/10.1021/acsomega.3c01231
ACS Omega 2023, 8, 20661−20674

Scheme 1. Possible Tautomeric Forms of 6MU and Their Relative Energies (kcal/mol, in Bold) Calculated by the m06-2x/cc-PVTZ Method

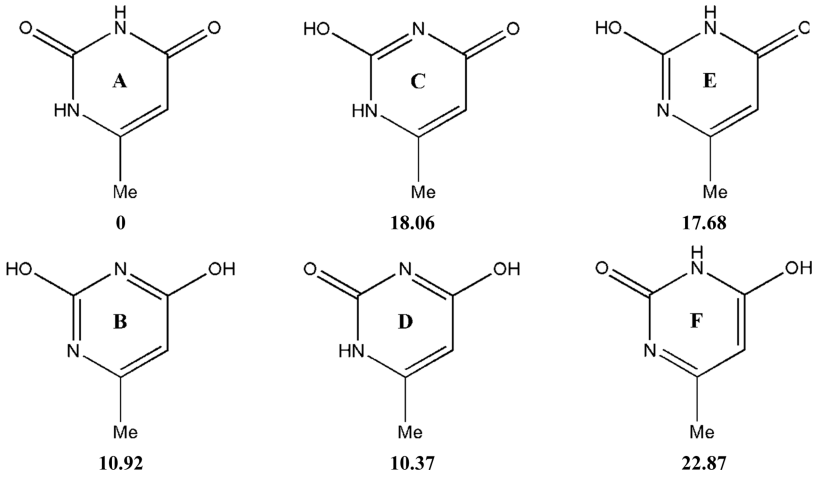

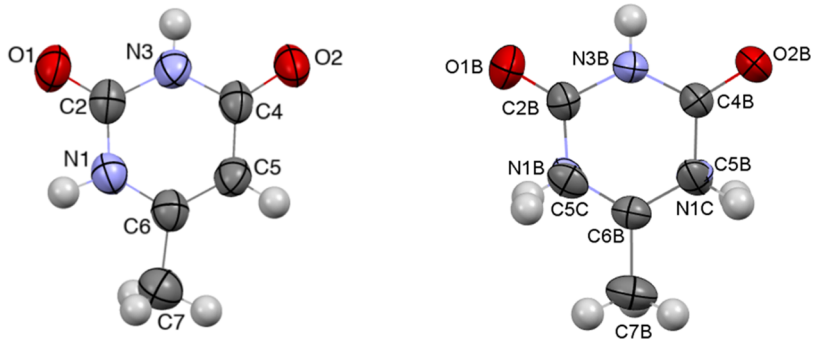

Figure 5. Molecular structure of **6MU** according to the X-ray diffraction data (on the left). The disordered molecule **B** found in the structure **6MU_IV** (on the right).

6MU_III. In contrast to the sublimation of the polymorphic form **6MU_I**, heating of **6MU_II** was not accompanied by the appearance of a white haze.

Characterization of 6MU Polymorphic Forms. *Powder Diffraction.* All of the separated individual polymorphic forms of **6MU** were characterized by the powder diffraction method (Figure 2). Rietveld refinement proved a nice agreement between the experimental diffractograms and the theoretical ones obtained from the single crystal study (Figure S1). The powder X-ray diffraction patterns of the polymorphs **6MU_I** and **6MU_III** with close unit cell parameters (Table 1) proved to be very similar (Figure 2). But the thorough analysis of these patterns has revealed some differences in the 2Θ region from 20 to 30° (Figure 3, and Tables S1 and S3). This fact allows to consider structure **6MU_III** as a new polymorphic form.

Differential Scanning Calorimetry (DSC). The pure polymorphic forms of **6MU** have been characterized by the DSC method (Figure 4). The **6MU_I** and **6MU_III** samples demonstrate the same melting process. The blue curve corresponded to polymorph **6MU_II** and has a wider melting band. The curve measured for the polymorphic form **6MU_IV** is very similar to the ones found for the samples of **6MU_I** and **6MU_III**. The similarity in DSC of **6MU_I** and **6MU_III** forms may be due to the similarity in the mutual arrangement of molecules and close energies of intermolecular interactions in their crystal structures.

Infrared Spectroscopy. The pure polymorphic forms of **6MU** have been characterized by infrared spectroscopy (Figures S2−S4 and Table S5) in the wavenumber range of 500−4000 cm^{-1} at room temperature. All of these spectra were measured with a resolution of 1 cm^{-1}. The analysis of infrared (IR) spectra has revealed the characteristic vibrations of the N−H bond in the regions of 3090−3040 and 2990−2938 cm^{-1}, vibrations of the CH_3 group in the region of 2850−2800 cm^{-1}. The carbonyl groups give vibrational lines in the regions of 1747−1704 and 1651−1644 cm^{-1} while the C═C bond is characterized by vibrations in the region of 1615−1614 cm^{-1}. Any vibrations corresponding to enol tautomers of **6MU** were not detected. The most significant changes are observed in the vibrational frequencies of the N−H bond (the region of 2850−2800 cm^{-1}) and carbonyl groups (Table S5), indicating different participation of the N1H and both carbonyl groups in hydrogen bonding. The vibrations of the methyl group and endocyclic double bond are very close in all polymorphic forms under study.

Molecular Structure Analysis. The **6MU** molecule can theoretically exist in six tautomeric forms (Scheme 1). According to the quantum chemical calculations using the MP2 electron correlated method, the diketo tautomeric form **A** proved to be the most stable.[22] Calculations by the m06-2x/cc-PVTZ method[26,27] coincide in general with the earlier data (Scheme 1) indicating that tautomer A is the most energetically preferable and tautomer F is the least expected. However, all possible tautomeric forms are expected to be in equilibrium

https://doi.org/10.1021/acsomega.3c01231
ACS Omega 2023, 8, 20661−20674

in a liquid or gas phase, and transitions between them can occur due to the transfer of a hydrogen atom. Which of these tautomeric forms can be found in a crystal phase depends on the crystallization conditions. It may be presumed that the kinetically controlled crystallization (rapid cooling of a supersaturated solution, rapid evaporation, sublimation, etc.) can lead to the formation of metastable polymorphic crystals containing a less energetically preferable tautomeric form or a mixture of several tautomers. Thermodynamically controlled crystallization should result in the formation of stable polymorphic crystals containing molecules in the tautomeric form with the lowest energy.

The positions of hydrogen atoms are usually determined not very reliably in an X-ray diffraction study. Consequently, the tautomeric form of a molecule in a crystal phase can be discussed mainly based on the analysis of bond lengths. Such an analysis was performed for **6MU** molecules in the polymorphic crystals **6MU_I**–**6MU_III**. An asymmetric part of the unit cell contains two molecules (**A** and **B**) in the **6MU_IV** structure, where molecule **B** is disordered over two positions with equal populations due to rotation around the virtual axis passing through the N3B···C6B atoms (Figure 5). To refine this disorder, the bond lengths in this molecule were restricted (see the Experimental Section). As a result, only bond lengths of molecule **A** may be analyzed in the **6MU_IV** polymorphic crystals.

The bond length analysis has revealed the diketo form of **6MU.** The C2–O1 and C4–O2 bonds have the same lengths (Table 3) in the polymorphic crystals **6MU_II**. This polymorph has been obtained from various solvents as a result of slow evaporation. The C═O bonds are not equivalent in **6MU** molecules found in all other structures (Table 3). Such a difference can be explained by two main reasons:

(a) contribution of zwitterionic forms to the molecular structure of **6MU** (Scheme 2);

(b) different participation of two carbonyl groups in intermolecular hydrogen bonds.

Table 3. Bond Lengths (Å) in the 6MU Molecule in Polymorphic Crystals 6MU_I – 6MU_IV

bond	6MU_I	6MU_II	6MU_III	6MU_IV[a]
N1–C2	1.372(4)	1.368(6)	1.353(5)	1.385(4)
C2–N3	1.370(4)	1.368(6)	1.381(6)	1.360(4)
N3–C4	1.370(4)	1.396(6)	1.378(5)	1.369(4)
C4–C5	1.417(5)	1.425(7)	1.400(6)	1.423(4)
C5–C6	1.337(5)	1.331(6)	1.353(6)	1.329(4)
C6–N1	1.362(4)	1.388(6)	1.384(5)	1.365(4)
C2–O1	1.215(4)	1.226(6)	1.230(5)	1.213(4)
C4–O2	1.253(4)	1.222(6)	1.253(6)	1.243(4)
C6–C7	1.497(5)	1.485(7)	1.469(6)	1.493(4)

[a]Bond lengths are presented for non-disordered molecule **A**.

The contribution of two zwitterionic structures to molecular geometry should slightly lengthen the C5–C6 bond and shorten the N3–C4, C4–C5, and N1–C6 bonds in **6MU** molecules found in structures **6MU_I**, **6MU_III**, and **6MU_IV**. The tendency for such a redistribution of electron density has been found in structures **6MU_I** and **6MU_III** and is absent in structure **6MU_IV** (Table 3). Therefore, the difference in bond lengths is caused mainly by the difference in the participation of carbonyl groups in intermolecular interactions. The higher ability of the C4–O2 carbonyl bond to be elongated can also be due to the stronger conjugation between the endocyclic C═C and exocyclic C═O double bonds compared to the conjugation between the electron lone pair of the nitrogen atom and the C═O bond.[28]

Crystal Structure Analysis. The analysis of intermolecular interactions in the polymorphic crystals under study has revealed different patterns formed by N–H···O hydrogen bonds in structures **6MU_I**, **6MU_III**, **6MU_IV**, and **6MU_II** (Figure 6). According to Etter's rules,[29,30] all strong proton donors and acceptors must participate in the formation of hydrogen bonds. The **6MU** molecule contains two NH groups and two carbonyl groups, which can form two strong centrosymmetric N–H···O hydrogen bonds. However, this rule is realized only in structure **6MU_II** while the N_3H donor and the C═O2 acceptor form a centrosymmetric dimer of the same type in all other crystals studied (Figure 6, Table 4).

Another NH group is also involved in intermolecular hydrogen bonding but with different acceptors in different polymorphic structures. The centrosymmetric dimer formed by the N1H and C═O1 groups is found only in the **6MU_II** structure. The centrosymmetric dimers of two types (formed by the N3–H···O2 or N1–H···O1 hydrogen bonds) form a ribbon as the main structural motif (Figure 6). The neighboring ribbons are bound by the weaker C–H···π hydrogen bonds (Table 4).

In structures **6MU_I**, **6MU_III**, and **6MU_IV**, the N1H group forms the linear intermolecular hydrogen bond with the C═O2 carbonyl group acting as a bifurcated proton acceptor. In addition, four centrosymmetric dimers bound by the N1–H···O2 hydrogen bonds form a cyclic fragment that can be recognized as a repeating part of the corrugated layer parallel to the (100) crystallographic plane in the structures **6MU_I** and **6MU_III** (Figure 6). The neighboring layers are bound by the weaker C5–H···O1 intermolecular hydrogen bonds.

In the **6MU_IV** polymorphic form, the centrosymmetric dimers formed due to the N3A–H···O2B and N3B–H···O2A hydrogen bonds between molecules **A** and **B** are bound by the linear N1A–H···O2B hydrogen bonds. So, a zigzag chain in the [010] crystallographic direction can be recognized as a

Scheme 2. Superposition of Resonance Structures Describing the 6MU Molecular Structure in Polymorphic Crystals 6MU_I, 6MU_III, and 6MU_IV

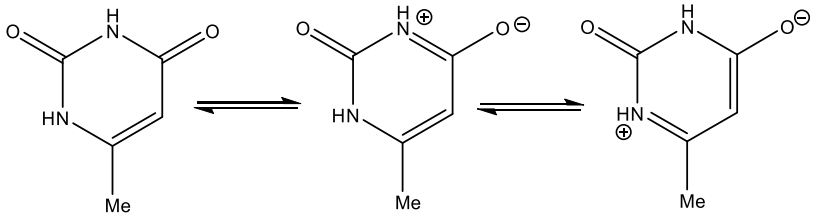

https://doi.org/10.1021/acsomega.3c01231
ACS Omega 2023, 8, 20661–20674

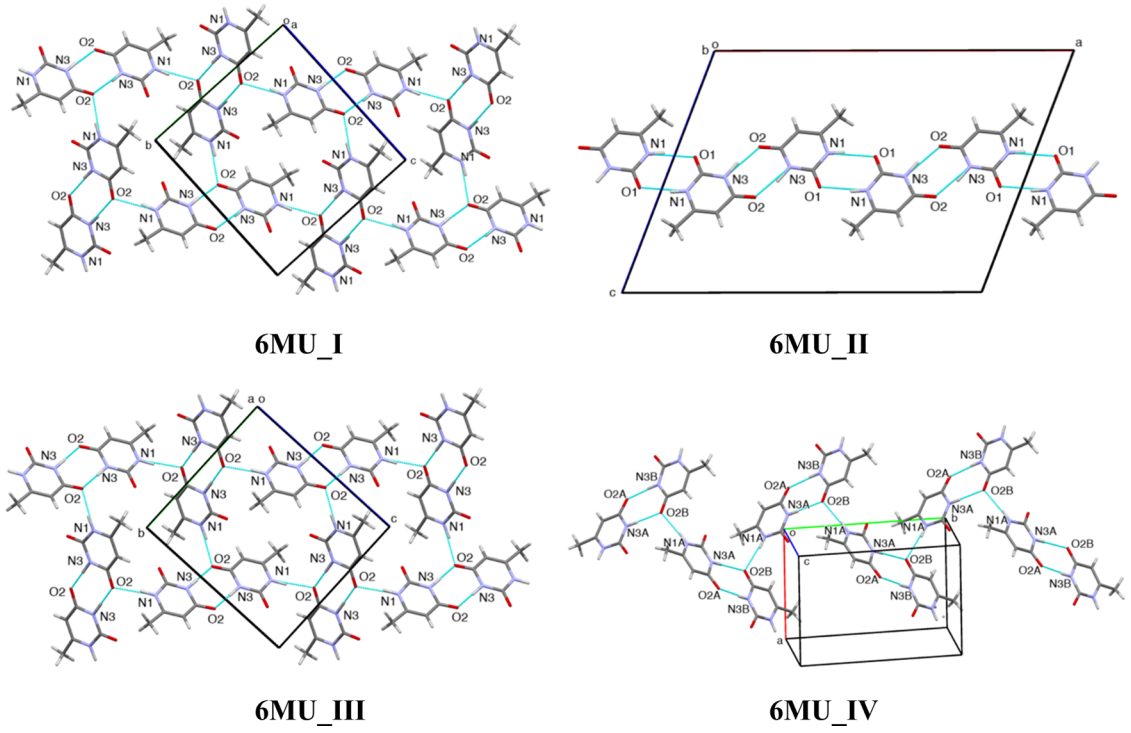

Figure 6. Packing patterns formed by the N−H···O intermolecular hydrogen bonds in the polymorphic structures of **6MU**.

structural motif in the polymorph **6MU_IV** (Figure 6). The disorder of molecule **B** in structure **6MU_IV** means the formation of hydrogen bonds of two types in one direction (N1C−H···O1A/C5B−H···O1A or N1B−H···O2A/C5C−H···O2A hydrogen bonds) linking the neighboring chains.

The energies of the hydrogen bonds revealed in four polymorphic crystals were estimated within Bader's "Atoms in Molecules" (AIM) theory.[31] The wave function for each of the hydrogen-bonded dimers was recorded by the m06-2x functional[26] and the standard cc-pVTZ basis set[27] (m06-2x/cc-pVTZ) and was analyzed using the AIM2000 program[32] with all default options. The energy of a hydrogen bond can be calculated using the correlation between the hydrogen bond energy and the pressure exerted on the electrons around the (3, −1) bond critical point revealed by Espinosa and co-workers.[33] The N3−H···O2′ intermolecular hydrogen bond proved to have the highest energy in all of the studied structures as compared to the N1−H···O1/O2 hydrogen bonds. This ratio persists even in the **6MU_II** polymorph (Table 4), where the N1−H···O1′ hydrogen bonds form a centrosymmetric dimer. The higher energy of the N3−H···O2 hydrogen bond is assumed to be a result of the higher ability of the C4═O2 bond to be delocalized. It should be noted that the smaller energy of the N3−H···O2′ hydrogen bond in **6MU_I** compared to **6MU_II** can be explained by the O2 participation in two hydrogen bonds simultaneously. The bifurcated character of N1−H···O2′ and N3−H···O2′ hydrogen bonds in **6MU_I** weakens both interactions.

The **6MU** molecule contains the conjugated system that creates pre-conditions for the formation of stacking interactions. The analysis of short contacts in the polymorphic structures **6MU_I** − **6MU_IV** has revealed the distances and overlapping degree between neighboring **6MU** molecules, which are characteristics of stacking. However, intermolecular interaction of this type is very complicated to be characterized.[34,35]

The analysis of pairwise interaction energies between neighboring molecules takes into account the contribution not only of hydrogen bonds but also stacking and non-specific interactions. Being more analytical and objective, such an analysis allows understanding the role of intermolecular interactions of different types in the crystal packing formation.[36] The first coordination sphere of the **6MU** molecule contains a different number of neighboring molecules in four polymorphic structures (Table 5). Furthermore, the highest interaction energy between a basic molecule and its first coordination sphere is found in polymorphic structure **6MU_II**, where the number of neighbors is the smallest. This may be explained by the presence of stronger hydrogen bonds between molecules forming a centrosymmetric dimer in the polymorphic form **6MU_II** (Table 5).

Based on our earlier data,[37,38] such interactions of a basic molecule with its environment allow presuming that the polymorphic form **6MU_II** is the most stable in comparison with other studied forms. The calculations of the lattice energies in periodic approximation for all of the polymorphic forms under study have revealed that polymorph **6MU_II** has the lowest lattice energy. The polymorphic structures **6MU_I**, **6MU_III**, and **6MU_IV** have lattice energies which are greater than 1.55, 1.53, and 1.67 kcal/mol, respectively. These data allow considering form **6MU_II** as stable while the forms **6MU_I**, **6MU_III**, and **6MU_IV** have to be recognized as metastable.

The basic molecule of **6MU** forms only one centrosymmetric dimer with the strongest interaction energy, but this dimer differs in the polymorphic structures **6MU_I**, **6MU_III**, **6MU_IV**, and **6MU_II** (Tables 5, and S6−S9). It is bound by the N3−H···O2 hydrogen bond in the structures **6MU_I**, **6MU_III**, and **6MU_IV** or by the N1−H···O1 hydrogen bond

https://doi.org/10.1021/acsomega.3c01231
ACS Omega 2023, 8, 20661−20674

Table 4. Intermolecular Interactions, Their Geometric Characteristics and Hydrogen Bond Energy, Evaluated from Characteristics of (3, −1) Bond Critical Point within the AIM Analysis in Polymorphic Crystals of 6MU

interaction	symmetry operation	geometric characteristics: H···A, Å	geometric characteristics: D−H···A, deg	E_{int}, kcal/mol (3, −1)
		6MU_I		
N1−H···O2′	x, 0.5 − y, −0.5 + z	1.94	168	−6.76
N3−H···O2′(2)	−x, −y, 1 − z	1.99	171	−11.42
C5−H···O1′	1 + x, 0.5 − y, 0.5 + z	2.40	174	−1.74
$\pi\cdots\pi$ stacking	x − 1, y, z	distance between planes 3.49 Å, shift 2.875 Å		
		6MU_II		
N1−H···O1′(2)	1 − x, −y, 1 − z	1.97	168	−12.39
N3−H···O2′(2)	1.5 − x, 0.5 − y, 1 − z	1.77	165	−22.57
C5−H···C4′	1.5 − x, 0.5 + y, 1.5 − z	2.82	170	−1.02
C5−H···C5′	1.5 − x, 0.5 + y, 1.5 − z	2.76	154	−0.98
$\pi\cdots\pi$ stacking	x, y − 1, z	distance between planes 3.33 Å, shift 2.049 Å		
		6MU_III		
N1−H···O2′	x, 0.5 − y, −0.5 + z	1.91	171	−8.52
N3−H···O2′(2)	−x, −y, 1 − z	1.77	176	−21.53
C5−H···O1′	1 + x, 0.5 − y, 0.5 + z	2.36	173	−1.92
$\pi\cdots\pi$ stacking	x − 1, y, z	distance between planes 3.49 Å, shift 3.009 Å		
		6MU_IV		
N1A−H···O2B′	−x, −0.5 + y, 0.5 − z	2.08	173	−4.42
N3A−H···O2B′	x, y, z	2.05	173	−12.58
C5A−H···O1B′	1 − x, −0.5 + y, 1.5 − z	2.45	159	−1.64
N1B−H···O2A′	x, 1.5 − y, −0.5 + z	2.21	169	−2.70
C5B−H···O1A′	1 + x, 1.5 − y, 0.5 + z	2.14	157	−3.83
N1C−H···O1A	1 + x, 1.5 − y, 0.5 + z	2.26	159	−2.32
C5C−H···O2A′	x, 1.5 − y, −0.5 + z	2.19	155	−3.29
$\pi\cdots\pi$ stacking (AB)	1 − x, 1 − y, 1 − z	distance between planes 3.25 Å, shift 2.675 Å		

Table 5. Number of Molecules Belonging to the First Coordination Sphere of the Basic 6MU Molecule, Total Interaction Energy of a Molecule with all Neighbors (kcal/mol) and a Hydrogen Bond in the Dimer with the Highest Interaction Energy

polymorph	number of neighbors	total E_{int}, kcal/mol	the dimer with the highest interaction energy: hydrogen bond	the dimer with the highest interaction energy: E_{int}, kcal/mol
6MU_I	16	−66.56	N3−H···O2(2)	−13.28
6MU_II	13	−67.12	N1−H···O1(2)	−19.31
6MU_III	14	−64.04	N3−H···O2(2)	−13.02
6MU_IV (A)	15	−65.56	N3−H···O2(2)	−13.20
6MU_IV (B)	14	−64.91		

in structure **6MU_II**. The question of which centrosymmetric dimer is the strongest in the structure **6MU_II** turned out to be somewhat controversial (Table 6).

According to the geometric characteristics, the N3−H···O2′ hydrogen bond is stronger than the N1−H···O1′ one. This is confirmed by the estimation of the hydrogen bond energy using the characteristics of the (3, −1) bond critical point within AIM analysis (Table 6). However, the interaction energy between two molecules in a centrosymmetric dimer bound by the N3−H···O2 bonds turned out to be smaller as compared to a similar dimer bound by the weaker N1−H···O1 bonds (Table S7). To resolve this contradiction, the interaction energies for two dimers bound by these hydrogen bonds were calculated using the m06-2x functional[26] with the TZVp basis set,[39] and their components were analyzed using the LMOEDA method[40] implemented in the GAMESS-US software package.[41] This analysis has shown that a stronger hydrogen bonding leads to an increase in energy of the electrostatic, exchange, polarization, and dispersion components of the total interaction energy (Table 6). In addition to the energy of the repulsive component increases to a greater extent due to an approach of molecules bound by the stronger N3−H···O2 hydrogen bonds. This results in a decrease in the total interaction energy between two molecules. This fact provides arguments in a long-standing controversy about what is the nature of the energy estimated from the characteristics of the (3, −1) bond critical point between two molecules bound by a hydrogen bond.[42,43] Is this the energy of interaction between contacting atoms or between molecules? Comparison of the energies of the N3−H···O2 and N1−H···O1 hydrogen bonds estimated from the (3, −1) bond critical points and the energies of interaction between molecules in the dimers bound by these hydrogen bonds (Table 6) suggests that the AIM theory provides the interaction energy between two contacting atoms rather than between two molecules.

The centrosymmetric dimer with the strongest interaction energy should be considered as a complex dimeric building unit (DBU_0) in all of the polymorphic **6MU** structures. The first coordination sphere of the DBU_0 contains the least amount of neighboring DBU_i in the **6MU_II** structure (Table 7). In addition, the total interaction energy with all surrounding is also the smallest in the **6MU_II** structure.

Structures **6MU_I** and **6MU_III** are very close (Figure 7). A basic DBU_0 forms four equal interactions (N1−H···O2 hydrogen bonds) in each of them (Table 8). As a result, the layer parallel to the (100) crystallographic plane may be recognized as BSM_1. The interaction energy of the DBU_0 with all neighboring DBU_i within the layer is −56.36 kcal in the **6MU_I** structure and −51.24 kcal/mol in the **6MU_III** structure. Neighboring layers are bound mainly by stacking interactions and C−H···O hydrogen bonds, and interaction energy between molecules belonging to neighboring layers is less than two times lower than the interaction energy within the layer (Table 7).

In the **6MU_II** structure, a DBU_0 also forms four dimers with neighboring DBU_i with very close energies (Table 8). But these dimers are not equivalent: two of them are bound by the N−H···O hydrogen bonds, and two more are bound by stacking interactions. Thus, the layer parallel to the (001) crystallographic plane and formed by interactions of two types, hydrogen bonding and stacking, can be recognized as BSM_1. The interaction energy of DBU_0 within the layer is −54.7 kcal/mol, while the interaction energy between neighboring layers is

https://doi.org/10.1021/acsomega.3c01231
ACS Omega 2023, 8, 20661−20674

Table 6. Comparison of the N3−H···O2 and N1−H···O1 Hydrogen Bonds Found in Structure 6MU_II: Geometric Characteristics, Interaction Energies within the Dimer and Their Components Calculated Using the LMOEDA Method and the Hydrogen Bond Energy Estimated from the (3, −1) Bond Critical Points within the AIM Theory

	geometric characteristics		interaction energy between two molecules and its components, kcal/mol						
hydrogen bond	H···A, Å	D−H···A, deg	E_{es},	E_{ex},	E_{rep},	E_{pol},	E_{disp},	total E_{int},	E_{hb}, (AIM), kcal/mol
N1-H···O1	1.97	168	−21.82	−9.25	29.11	−7.28	−8.52	−17.75	−12.39
N3-H···O2	1.77	165	−24.41	−18.31	53.12	−13.64	−10.94	−14.19	−22.57

Table 7. Interaction Energies (in kcal/mol) of a DBU_0 with Its First Coordination Sphere, within Recognized Basic Structural Motifs and between Them in Polymorphic 6MU Structures

polymorphic form	number of neighboring DBU	E_{int} (total), kcal/mol	BSM_1	E_{int} (BSM_1), kcal/mol	E_{int} (BSM_1/BSM_1), kcal/mol
6MU_I	17	−105.88	layer	−50.36	−27.47
6MU_II	16	−92.21	layer	−54.70	−14.67
6MU_III	18	−109.07	layer	−51.24	−29.97
6MU_IV	17	−104.77	corrugated layer	−47.78	−38.37

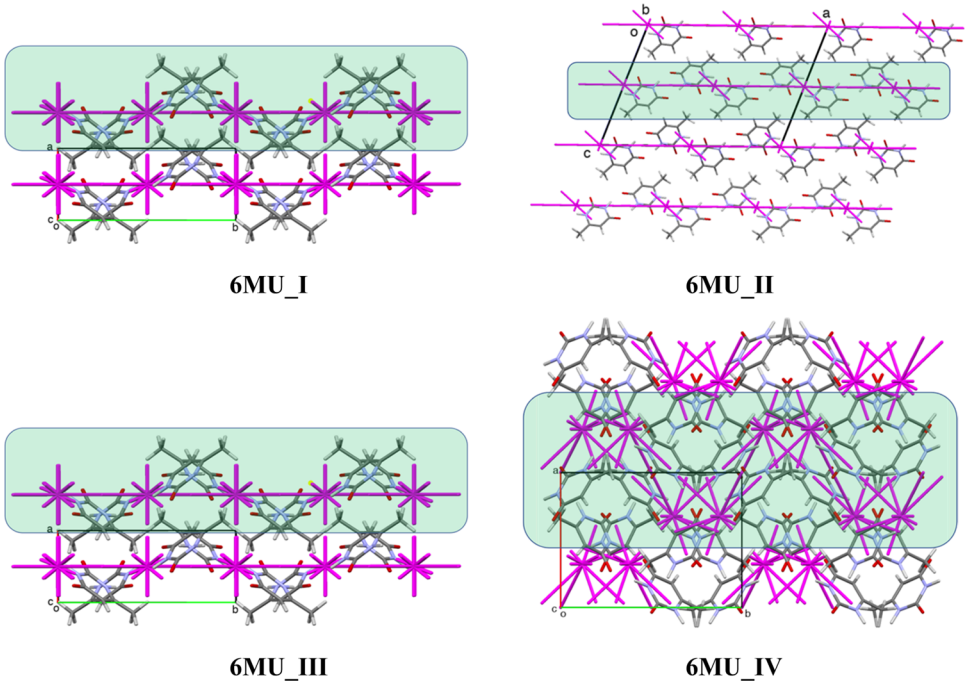

Figure 7. Packing of **6MU** in terms of molecules and energy-vector diagrams of DBU (in purple) in the studied polymorphic forms. The layers are selected and highlighted in green.

only −14.67 kcal/mol. It should be concluded that the **6MU_II** structure is also layered, similar to the **6MU_I** and **6MU_III** structures, but this polymorph has a much more anisotropic structure in terms of the interaction energies between molecules (Figure 7 and Table 7).

In the **6MU_IV** structure, the strongest interaction between dimeric BUs is the stacking, which proved to be slightly stronger than the N−H···O hydrogen bonds (Table 8). The formation of three interactions with comparable energies results in the packing that is much more isotropic as compared to the polymorphic forms **6MU_I** − **6MU_III**. A very corrugated layer parallel to the (100) crystallographic plane may be recognized as a BSM_1 in the **6MU_IV** structure (Figure 7), but the interaction energies of DBU_0 with its neighbors within this layer and with DBU_i belonging to neighboring layers are very close (Table 7).

Comparison of the structures and crystallization conditions of all **6MU** polymorphs showed some regularities observed earlier for crystals obtained as a result of a kinetically or thermodynamically controlled crystallization process.[38,44] Crystallization under nonequilibrium conditions (stirring a solution or sublimation from a solid) results in crystals with lower density and more isotropic energies of interactions between molecules (structures **6MU_I**, **6MU_III**, and **6MU_IV**). Slow crystallization from a solution under ambient conditions leads to a crystal structure with a higher density and more anisotropic energies of interactions (the **6MU_II** structure).

It should be noted that the metastable polymorph **6MU_I** is used in the pharmaceutical industry, and two new metastable forms, **6MU_III** and **6MU_IV**, can be formed during the technological process due to temperature violations. Therefore, the question of their behavior under mechanical stress or pressure is of great practical importance. To estimate the possibility of a polymorphic transition under external influence in these metastable polymorphic forms, the method proposed

https://doi.org/10.1021/acsomega.3c01231
ACS Omega 2023, 8, 20661−20674

Table 8. Symmetry Codes, Bonding Type, and Interaction Energies of the DBU_0 with Neighbors (E_{int}, kcal/mol) with the Highest Values (More Than 5% of the Total Interaction Energy), and the Contribution of These Energies to the Total Interaction Energy (%) in the 6MU Polymorphic Structures

dimer DBU_0-DBU_i	symmetry operation	E_{int}, kcal/mol	contribution to the total interaction energy, %	bonding type
		6MU_I		
dd1	$1 - x, 1/2 + y, -1/2 - z$	−12.59	11.9	N−H···O
dd2	$1 - x, -1/2 + y, 1/2 - z$	−12.59	11.9	N−H···O
dd3	$1 - x, 1/2 + y, 1/2 - z$	−12.59	11.9	N−H···O
dd4	$1 - x, -1/2 + y, -1/2 - z$	−12.59	11.9	N−H···O
dd5	$1 + x, y, z$	−10.17	9.6	stacking
dd6	$-1 + x, y, z$	−10.17	9.6	stacking
		6MU_II		
dd1	$1/2 + x, -1/2 + y, z$	−13.70	14.9	N−H···O
dd2	$-1/2 + x, 1/2 + y, z$	−13.70	14.9	N−H···O
dd3	$x, 1 + y, z$	−13.65	14.8	stacking
dd4	$x, -1 + y, z$	−13.65	14.8	stacking
dd5	$-1/2 - x, 1/2 + y, -1/2 - z$	−6.12	6.6	C−H···π
dd6	$1/2 - x, -1/2 + y, 1/2 - z$	−6.12	6.6	C−H···π
dd7	$-1/2 - x, -1/2 + y, -1/2 - z$	−6.12	6.6	C−H···π
dd8	$1/2 - x, 1/2 + y, 1/2 - z$	−6.12	6.6	C−H···π
		6MU_III		
dd1	$1 - x, 1/2 + y, -1/2 - z$	−12.81	11.7	N−H···O
dd2	$1 - x, -1/2 + y, 1/2 - z$	−12.81	11.7	N−H···O
dd3	$1 - x, 1/2 + y, 1/2 - z$	−12.81	11.7	N−H···O
dd4	$1 - x, -1/2 + y, -1/2 - z$	−12.81	11.7	N−H···O
dd5	$1 + x, y, z$	−10.80	9.9	stacking
dd6	$-1 + x, y, z$	−10.80	9.9	stacking
		6MU_IV		
dd1	$-x, 1 - y, 1 - z$	−14.23	13.6	stacking
dd2	$-x, -1/2 + y, 1/2 - z$	−12.78	12.2	N−H···O
dd3	$-x, 1/2 + y, 1/2 - z$	−12.78	12.2	N−H···O
dd4	$1 - x, -y, 1 - z$	−9.16	8.7	non-specific
dd5	$-1 + x, 1/2 - y, -1/2 + z$	−7.99	7.6	N−H···O
dd6	$1 + x, 1/2 - y, 1/2 + z$	−7.99	7.6	N−H···O
dd7	$1 - x, 1 - y, 1 - z$	−7.48	7.1	non-specific

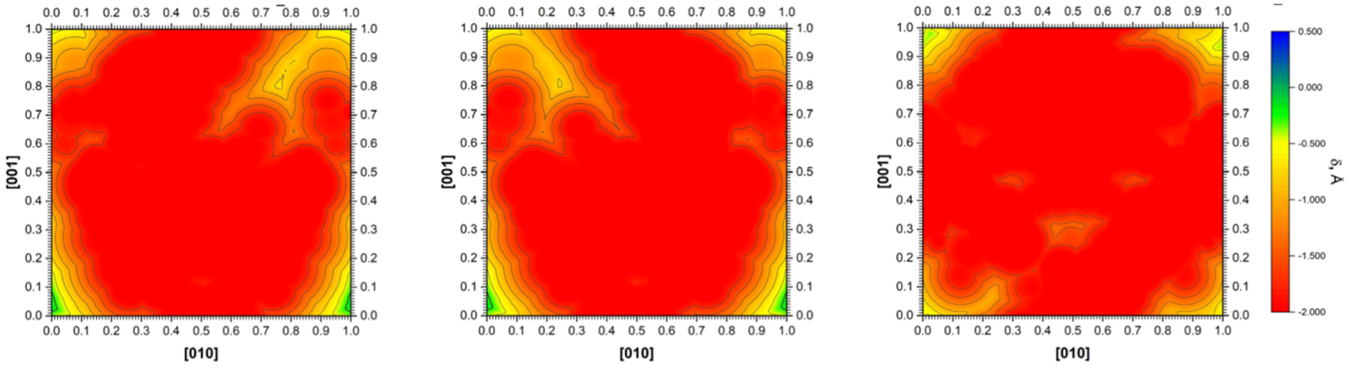

Figure 8. Maps of δ (Å) occurring during the shear of the dimeric mobile part in relation to the fixed part in the (100) plane (directions of the shift are shown by axes) in the metastable polymorphic **6MU_I** crystals (on the left panel), **6MU_III** (in the center panel), and **6MU_IV** (on the right panel).

earlier[45−47] was applied. The results of the study of pairwise interaction energies in metastable polymorphic forms can be used to determine a possible way of the crystal structure deformation. All of these structures are layered where interaction energies between DBUs within the layer are high and interactions between layers are weak. Therefore, it may be assumed that one layer can be shifted in relation to the neighboring one as a result of mechanical stress or pressure exerted on a crystal. The displacement of the neighboring layers can be modeled using the model system where the fragment of a layer plays the role of a fixed part and one DBU belonging to the neighboring layer acts as a mobile part. The molecule of **6MU** is conformationally rigid, which allows us to use the rigid body model. The displacement of the mobile part in relation to the fixed part with some step models a possible structure deformation. To evaluate the probability of this process, it is sufficient at the first stage to measure at each point the closest distances between atoms belonging to the

https://doi.org/10.1021/acsomega.3c01231
ACS Omega 2023, 8, 20661−20674

fixed and mobile parts of the model system. These distances should be compared with the sums of the van der Waals radii of the corresponding atom in order to take into account the nature of the closest atoms. The parameter δ calculated as the difference between the shortest distance and the corresponding van der Waals radius sum during the displacement of the mobile part relative to the fixed part can be used to construct two-dimensional (2D) maps (Figure 8).

Such 2D maps constructed for the displacements along the (100) crystallographic plane in the metastable structures **6MU_I**, **6MU_III**, and **6MU_IV** (Figure 8) clearly show that any deformation of the studied crystal structures leads to a significant shortening of the distances between the closest atoms belonging to molecules of the mobile and fixed parts of the model system that causes the appearance of strong repulsion. As a result, any polymorphic transition without the loss of crystallinity looks impossible. Thus, it can be concluded that the metastable polymorphic forms of **6MU** have to be resistant to any external influences during the technological process.

CONCLUSIONS

A thorough study of crystalline forms of 6-methyluracil (**6MU**), which affects the regulation of lipid peroxidation and wound healing, leads to finding of two new polymorphic modifications that can be formed in the technological process due to temperature violations. For two previously known and two new polymorphic modifications, the conditions for their preparation were studied. The structure of all polymorphic modifications of **6MU** was unambiguously established by the single crystal X-ray diffraction study. The obtained crystalline forms have also been characterized by the powder X-ray diffraction method, differential scanning calorimetry method, and IR spectroscopy.

The calculations of pairwise interactions between molecules, as well as calculations of the lattice energies in periodic approximation, have shown that the **6MU_II** polymorphic form is the most stable, while the **6MU_I** form used in the pharmaceutical industry and the new forms **6MU_III** and **6MU_IV**, which can be formed by sublimation, are metastable. In all of the polymorphic modifications, the centrosymmetric dimer formed by two N−H···O hydrogen bonds between **6MU** molecules is a dimeric building unit (DBU) of the crystal structure. The calculations of pairwise interaction energies between DBUs have revealed that the studied crystalline forms have a layered structure. The comparison of interaction energies of DBU_0 with its neighbors within the layer and with ones belonging to neighboring layers allows us to conclude that the most stable **6MU_II** form has the most anisotropic "energetic" structure. The interaction energy of DBU_0 with its neighbors within the layer parallel to the (001) crystallographic plane, is more than three times higher than the interaction energy with the molecules of the neighboring layer. The metastable polymorphic forms of **6MU** obtained under more nonequilibrium conditions (stirring or sublimation) have a much more isotropic "energetic" structure. The interaction energy of DBU_0 with its neighbors within the layer parallel to the (100) crystallographic plane is almost two times higher than with the molecules of the neighboring layer in the **6MU_I** and **6MU_III** structures. In the most unstable polymorph **6MU_IV**, the layer is highly corrugated, and the energies of DBU_0 interactions within the layer and with the adjacent layer are very close.

The pharmaceutical industry uses the metastable polymorphic form **6MU_I** and two new metastable forms, **6MU_III** and **6MU_IV**, which may be formed during the technological process. Therefore, the possibility of these structures to be deformed under external influence such as mechanical stress or pressure during tableting was evaluated using quantum chemical modeling. It was shown that any structure deformation leads to a significant decrease in the distances between the closest atoms belonging to the neighboring layers. This fact allows to conclude that the metastable polymorphic forms of **6MU** cannot undergo a polymorphic transition under external influence and can be used in the technological process without any limitations.

EXPERIMENTAL SECTION

Materials and Crystallization. 6-Methyluracil (**6MU**) was purchased from the pharmaceutical company JSC "Farmak". The solvents used were purchased from Sigma and were of analytical grade. **6MU** was crystallized from different solvents (methanol, ethanol, isopropyl, isoamyl alcohol, acetonitrile, water, ethyl acetate, DMF, DMSO). Each solvent (10 mL) was used to dissolve a sample of **6MU** (20 mg). The mixtures were blended and heated until clear solutions were obtained. The solutions were cooled slowly and left for slow evaporation at room temperature. Crystals suitable for X-ray diffraction analysis were obtained after some days according to the evaporation rate of the corresponding solvent.

Crystallization due to sublimation of a crystal sample was also used. A sample of **6MU** was placed in a thermally resistant beaker covered with a glass slide and heated. Crystals suitable for an X-ray diffraction study were obtained on the interior side of the glass slide.

X-ray Diffraction. *Single Crystal X-ray Diffraction.* The single crystal X-ray diffraction study was performed on an "Xcalibur-3" diffractometer (graphite monochromated Mo Kα radiation (λ = 0.71073), CCD detector, ω-scans). The structures were solved by a direct method and refined against F^2 within anisotropic approximation for all non-hydrogen atoms using the OLEX2 program package[48] with SHELXT[49] and SHELXL modules.[50] The twin law in structure **6MU_IV** was identified using the TwinRotMat routine in PLATON.[51] The two twin components are related by 2-fold rotation about the *b*-axis, with refined major to minor occupancy fractions of 0.783(1):0.217(1). The bond lengths in a disordered **6MU** molecule found in polymorph **IV** were restricted with values of 1.372 Å for the $Csp^2(=O)-N$ bond, 1.362 Å for the Csp^2-N bond, 1.337 Å for the $Csp^2=Csp^2$ bond. Hydrogen atoms were located in electron density difference maps, and those bonded to N atoms were refined freely in structures **6MU_I**, **6MU_II**, and **6MU_III**. The positions of the hydrogen atoms in the CH and CH_3 groups in all of the studied structures as well as the NH groups in the structure **6MU_IV** were refined using a riding model, with $U_{iso} = nU_{eq}$ (n = 1.5 for the methyl group and 1.2 for other atoms) parameter set of the parent atoms.

Powder X-ray Diffraction. The powder X-ray diffraction (PXRD) study was carried out with a Siemens D500 powder diffractometer at room temperature (Cu Kα radiation, Bragg−Brentano geometry, curved graphite monochromator on the counter arm, 5 < 2 θ < 60°, $\Delta 2\theta$ = 0.02°). The initial processing of the obtained PXRD patterns was performed using the PowderX program.[52] The FullProf&WinPLOTR program[53] was used for Rietveld refinement. An Al_2O_3 plate

https://doi.org/10.1021/acsomega.3c01231
ACS Omega 2023, 8, 20661−20674

(NIST SRM1976) was used as the external standard, and to determine the instrumental profile function. The Rietveld refinement of the PXRD patterns for obtaining the temperature relationships of the cell dimensions was performed using a rigid body model (as implemented in the FullProf program) of the **6MU** molecule taken from single crystal results.

Differential Scanning Calorimetry (DSC). DSC analysis was carried out using a TA Instrument Q2000. The sample is continuously purged with 50 mL/min nitrogen (99.999%). About 1−2 mg of the **6MU** powder was crimped in an aluminum standard sample pan with a lid. For each analysis, a new sample was prepared. The heating rate was 5 °C/min.

Infrared Spectroscopy. Mid-infrared absorption spectra were acquired with a Nicolet IS 50 Fourier transform infrared (FT-IR) spectrometer with ATR. The spectrophotometer has a diamond ATR crystal, KBr beam splitter, and KBr DTGS detector.

Quantum Chemical Study. *Molecular Structure Study.* The optimization of all of the possible tautomeric forms of **6MU** was performed using density functional theory with the m06-2x functional[26] and the standard cc-pVTZ basis set[27] (m06-2x/cc-pVTZ). The character of the stationary points on the potential energy surface was verified by calculations of vibrational frequencies within the harmonic approximation using analytical second derivatives at the same level of theory. All minima on PES possess zero imaginary frequencies. All calculations were performed using the Gaussian09 program.[54]

Analysis of the Interaction Energy Components. The interaction energies in two centrosymmetric dimers bound by N3−H···O2 or N1−H···O1 hydrogen bonds in the **6MU_II** polymorph were calculated by the m06-2x/TZVp method.[26,39] The interaction energy components were analyzed using the LMOEDA method.[40] The GAMESS-US software[41] was used for these calculations.

Crystal Structure Analysis from the Energetic Viewpoint. The analysis of the "energetic" structure was performed using the approach based on quantum chemical calculations of pairwise interaction energies between molecules.[55,56] According to this method, a molecule (monomeric building unit, MBU) or strongly bound dimer of molecules (dimeric building unit, DBU) may be considered as a basic building unit (BU_0) of a crystal structure. The first coordination sphere of BU_0 can be constructed using a standard procedure within the Mercury program.[57] The first coordination sphere includes all molecules or dimers for which the distance between atoms of the basic BU_0 and its symmetrically equivalent BU_i is shorter than the corresponding van der Waals radii sum plus 1 Å at least for one pair of atoms. The fragment of a crystal packing separated in such a way was divided into dimers BU_0-BU_i without any change in their geometry. X−H bonds are shortened in the X-ray diffraction study,[58] therefore, the positions of hydrogen atoms were normalized to 1.089 Å for C−H and 1.015 Å for N−H bonds according to the neutron diffraction data.[59] The pairwise interaction energies for the BU_0-BU_i dimers were calculated using the B97D3 density functional method[60,61] and def2-TZVP basic set.[62,63] All of the calculated energies were corrected for a basis set superposition error by the counterpoise method.[64] The choice of the calculation method was based on the benchmark study of an accurate estimation of pairwise interaction energies.[65] All of the single-point calculations were performed within the ORCA program.[66] The obtained data were visualized using energy-vector diagrams (EVD) proposed earlier.[56]

Calculations in Periodic Approximation. The calculations of the lattice energies were performed in periodic boundary conditions using the Quantum ESPRESSO program.[67] The pseudopotential PAW method with the PBE exchange-correlated functional was applied. The plane-wave cut-off energies and cut-off electronic change density were used as 45 and 225 Ry for all calculations. The atomic coordinates of the four structures were optimized using the "vc-relax" routine embedded in the software.

Modeling of Shear Deformation Possibility. For modeling the shear deformation possibility, DBU_0 (mobile part) and a fragment of the neighboring layer (fixed part) were extracted from the crystal structure.[46,47] The displacement of the mobile part in relation to the fixed part on one crystallographic translation in two directions within the layer fragment was performed with the step size equal to 1/100 of a translation. The minimal interatomic distances between molecules of the mobile and fixed parts were calculated at each point of the displacement. The difference of interatomic distances and corresponding van der Waals radii sum (parameter δ) was used to take into account the nature of the nearest atoms belonging to the mobile and fixed parts of a model system

$$\delta_{ij} = d_{ij} - vdW_i - vdW_j \quad (1)$$

where d_{ij}, vdW_i, and vdW_j are the distance between the atoms i in the mobile part and j in the fixed part and their van der Waals radii, respectively.

A decrease in the parameter δ compared to the initial point indicates the appearance of steric repulsion between the mobile and fixed parts of the model system, which prevents any structure deformation.

■ ASSOCIATED CONTENT

Supporting Information

The Supporting Information is available free of charge at https://pubs.acs.org/doi/10.1021/acsomega.3c01231.

Tables with full PXRD and IR-spectroscopy data; full tables of the pairwise interaction energies between building units (molecular and dimeric); figures of final Rietveld plots, IR spectrum, and crystal packing along different crystallographic directions in terms of molecules and energy-vector diagrams (PDF)

■ AUTHOR INFORMATION

Corresponding Author

Svitlana V. Shishkina − *SSI "Institute for Single Crystals" NAS of Ukraine, Kharkiv 61001, Ukraine; V. N. Karazin Kharkiv National University, Kharkiv 61022, Ukraine;* orcid.org/0000-0002-3946-1061; Phone: +38 066 771 87 42; Email: sveta12.20@gmail.com, sveta@xray.isc.kharkov.com

Authors

Anna M. Shaposhnik − *SSI "Institute for Single Crystals" NAS of Ukraine, Kharkiv 61001, Ukraine*

Victoriya V. Dyakonenko − *SSI "Institute for Single Crystals" NAS of Ukraine, Kharkiv 61001, Ukraine*

Vyacheslav M. Baumer − *SSI "Institute for Single Crystals" NAS of Ukraine, Kharkiv 61001, Ukraine*

Vitalii V. Rudiuk − *Farmak JSC, Kyiv 04080, Ukraine*

Igor B. Yanchuk − *Farmak JSC, Kyiv 04080, Ukraine*

https://doi.org/10.1021/acsomega.3c01231
ACS Omega 2023, 8, 20661−20674

Igor A. Levandovskiy − *Department of Organic Chemistry, National Technical University of Ukraine "Igor Sikorsky Kyiv Polytechnic Institute", 03056 Kyiv, Ukraine*

Complete contact information is available at: https://pubs.acs.org/10.1021/acsomega.3c01231

Author Contributions

S.S. performed quantum chemical calculations, analyzed the results, and wrote the manuscript; A.S. performed RXRD studies; V.D. modeled the possible shear deformations; V.B. performed Rietveld refinement; V.R. crystallized the compound and discussed the results; I.Y. performed DSC and IR-spectroscopy studies; I.L. performed calculations in periodic boundary conditions.

Notes

The authors declare no competing financial interest.

REFERENCES

(1) Bernstein, J. *Polymorphism in Molecular Crystals*; Clarendon Press: Oxford, 2002.
(2) Brittain, H. G. *Polymorph in Pharmaceutical Solids*, 2nd ed.; Brittain, H. G., Ed.; Informa Healthcare: Oxford, 2009; pp 1−23.
(3) Lee, A. Y.; Erdemir, D.; Myerson, A. S. Crystal polymorphism in chemical process development. *Annu. Rev. Chem. Biomol. Eng.* **2011**, *2*, 259−280.
(4) Censi, R.; Di Martino, P. Polymorph impact on the bioavailability and stability of poorly soluble drugs. *Molecules* **2015**, *20*, 18759−18776.
(5) Von Raumer, M.; Hilfiker, R. Solid state and polymorphism of the drug substance in the context of quality by design and ICH Guidelines Q8−Q12. In *Polymorphism in the Pharmaceutical Industry*; Hilfiker, R.; Von Raumer, M., Eds.; Wiley-VCH: Weinheim, 2019; pp 1−30.
(6) Lu, J.; Rohani, S. Polymorphism and crystallization of active pharmaceutical ingredients (APIs). *Curr. Med. Chem.* **2009**, *16*, 884−905.
(7) Guthrie, S. M.; Smilgies, D.-M.; Giri, G. Controlling polymorphism in pharmaceutical compounds using solution shearing. *Cryst. Growth Des.* **2018**, *18*, 602−606.
(8) Hilfiker, R.; Blatter, F.; Raumer, M. Relevance of Solid-State Properties for Pharmaceutical Products. In *Polymorphism in the Pharmaceutical Industry*; Hilfiker, R., Ed.; Wiley-VCH: Weinheim, 2006; pp 1−19.
(9) Chemburkar, S. R.; Bauer, J.; Deming, K.; Spiwek, H.; Patel, K.; Morris, J.; Henry, R.; Spanton, S.; Dziki, W.; Porter, W.; Quick, J.; Bauer, P.; Donaubauer, J.; Narayanan, B. A.; Soldani, M.; Riley, D.; McFarland, K. Dealing with the impact of ritonavir polymorphs on the late stages of bulk drug process development. *Org. Process Res. Dev.* **2000**, *4*, 413−417.
(10) Santos, O. M. M.; Reis, M. E. D.; Jacon, J. T.; Lino, M. E. S.; Simões, J. S.; Doriguetto, A. C. Polymorphism: an evaluation of the potential risk to the quality of drug products from the farmácia popular rede própria. *Braz. J. Pharm. Sci.* **2014**, *50*, 1−24.
(11) Groom, C. R.; Bruno, I. J.; Lightfoot, M. P.; Ward, S. C. The Cambridge Structural Database. *Acta Crystallogr., Sect. B: Struct. Sci., Cryst. Eng. Mater.* **2016**, *72*, 171−179.
(12) Chennuru, R.; Muthudoss, P.; Ramakrishnan, S.; Mohammad, A. B.; Babu, R. R. C.; Mahapatra, S.; Nayak, S. K. Preliminary studies on unusual polymorphs of thymine: Structural comparison with other nucleobases. *J. Mol. Struct.* **2016**, *1120*, 86−99.
(13) Braun, D. E.; Gelbrich, T.; Wurst, K.; Griesser, U. J. Computational and experimental characterization of five crystal forms of thymine: packing polymorphism, polytypism/disorder, and stoichiometric 0.8-hydrate. *Cryst. Growth Des.* **2016**, *16*, 3480−3496.
(14) Zee-Cheng, K.-Y.; Robins, R. K.; Cheng, C. C. Pyrimidines. III. 5,6-Dihydropyrimidines. *J. Org. Chem.* **1961**, *26*, 1877−1884.
(15) Bhat, K. S.; Rao, A. S. Synthesis of uracil, 6-methyluracil and some dihydrouracils. *Org. Prep. Proced. Int.* **1983**, *15*, 303−312.
(16) Taran, Iu. P.; Shishkina, L. N. Effect of 6-methyluracil on various indicators of the lipid peroxidation regulation system in the body. *Vopr. Med. Khim.* **1993**, *39*, 37−41.
(17) Taran, Yu. P.; Shishkina, L. N.; Evseenko, L. S.; Kukushkina, G. V. Effect of 6-methyluracil on regulatory parameters of lipid peroxidationin thermal burn. *Patol. Fiziol. Eksp. Ter.* **1995**, *1*, 40−43.
(18) Oksman, A. Y. Method of prevention of lysosomal leakage in eukaryotic cells by using 6-methyluracil based water-soluble compounds and method of producing thereof. U.S. Patent US2005/0064382 A1, 2005.
(19) Oksman, A. Y. Method of prevention of lysosomal leakage in eukaryotic cells by using 6-methyluracil based water-soluble compounds and method of producing thereof. U.S. Patent US2005/0207541 A1, 2007.
(20) Reck, G.; Kretschmer, R.-G.; Kutschabsky, L.; Pritzkow, W. *POSIT* − a method for structure determination of small partially known molecules from powder diffraction data. Structure of 6-methyl-1,2,3,4-tetrahydropyrimidine-2,4-dione (6-methyluracil). *Acta Crystallogr., Sect. A: Found. Crystallogr.* **1988**, *A44*, 417−421.
(21) Naumov, V. A. Molecular structure of 6-methyluracil in the gas phase and characteristics of the 6-methyluracil-water system. *Russ. J. Gen. Chem.* **2008**, *78*, 432−438.
(22) Lukmanov, T.; Ivanov, S. P.; Khamitov, E. M.; Khursan, S. L. Relative stability of keto-enol tautomers in 5,6-substituted uracils: ab initio, DFT and PCM study. *Comput. Theor. Chem.* **2013**, *1023*, 38−45.
(23) Leonidov, N. B.; Zorkii, P. M.; Masunov, A. E.; Gladkikh, O. P.; Bel'skii, V. K.; Dzyabchenko, A. V.; Ivanov, S. A. The structure and biological nonequivalence of methyluracil polymorphs. *Russ. J. Phys. Chem.* **1993**, *67*, 2220−2223.
(24) Portalone, G. 6-Methyluracil: a redetermination of polymorph (II). *IUCrData* **2019**, *4*, No. x190861.
(25) Leonidov, N. B.; Obukhova, L. K.; Okladnova, O. V.; Romanenko, E. B. Effect of polymorphic forms of methyluracil on the development and lifespan of *Drosophila melanogaster*. *Bull. Exp. Biol. Med.* **1999**, *127*, 603−606.
(26) Zhao, Y.; Truhlar, D. G. The M06 suite of density functionals for main group thermochemistry, thermochemical kinetics, noncovalent interactions, excited states, and transition elements: two new functionals and systematic testing of four M06-class functionals and 12 other functionals. *Theor. Chem. Acc.* **2007**, *120*, 215−241.
(27) Kendall, R. A.; Dunning, T. H., Jr.; Harrison, R. J. Electron affinities of the first-row atoms revisited. Systematic basis sets and wave functions. *J. Chem. Phys.* **1992**, *96*, 6796−6806.
(28) Kirby, A. J. *Stereoelectronic Effects*; Oxford University Press: Oxford, 1996.
(29) Etter, M. C. Encoding and decoding hydrogen-bond patterns in organic compounds. *Acc. Chem. Res.* **1990**, *23*, 120−126.
(30) Etter, M. C. Hydrogen bonds as design elements in organic chemistry. *J. Phys. Chem. A* **1991**, *95*, 4601−4610.
(31) Bader, R. F. W. *Atoms in Molecules: a Quantum Theory*; Oxford University Press: Oxford, 1990.
(32) Biegler-Konig, F.; Schonbohm, J.; Bayles, D. AIM2000-A program to analyze and visualize atoms in molecules. *J. Comput. Chem.* **2001**, *22*, 545−559.
(33) Espinosa, E.; Molins, E.; Lecomte, C. Hydrogen bond strengths revealed by topological analyses of experimentally observed electron densities. *Chem. Phys. Lett.* **1998**, *285*, 170−173.
(34) Zhikol, O. A.; Shishkin, O. V.; Lyssenko, K. A.; Leszczynski, J. Electron density distribution in stacked benzene dimers: a new approach towards the estimation of stacking interaction energies. *J. Chem. Phys.* **2005**, *122*, No. 144104.
(35) Spackman, M. A. How reliable are intermolecular interaction energies estimated from topological analysis of experimental electron densities? *Cryst. Growth Des.* **2015**, *15*, 5624−5628.
(36) Shishkin, O. V.; Zubatyuk, R. I.; Shishkina, S. V.; Dyakonenko, V. V.; Medviediev, V. V. Role of supramolecular synthons in the

formation of the supramolecular architecture of molecular crystals revisited from an energetic viewpoint. *Phys. Chem. Chem. Phys.* **2014**, *16*, 6773−6786.
(37) Shishkina, S. V.; Konovalova, I. S.; Karpina, V. R.; Kovalenko, S. S.; Kovalenko, S. M.; Bunyatyan, N. D. Concomitant polymorphic forms of 3-cyclopropyl-5-(2-hydrazinylpyridin-3-yl)-1,2,4-oxadiazole. *Acta Crystallogr., Sect. C: Struct. Chem.* **2020**, *76*, 836−844.
(38) Shishkina, S. V.; Baumer, V. N.; Kovalenko, S. M.; Trostianko, P. V.; Bunyatyan, N. D. Usage of quantum chemical methods to understand the formation of concomitant polymorphs of acetyl 2-(*N*-(2-fluorophenyl)imino)coumarin-3-carboxamide. *ACS Omega* **2021**, *6*, 3120−3129.
(39) Schäfer, A.; Huber, C.; Ahlrichs, R. Fully optimized contracted Gaussian-basis sets of triple zeta valence quality for atoms Li to Kr. *J. Chem. Phys.* **1994**, *100*, 5829−5835.
(40) Su, P.; Li, H. Energy decomposition analysis of covalent bonds and intermolecular interactions. *J. Chem. Phys.* **2009**, *131*, No. 014102.
(41) Schmidt, M. W.; Baldridge, K. K.; Boatz, J. A.; Elbert, S. T.; Gordon, M. S.; Jensen, J. H.; Koseki, S.; Matsunaga, N.; Nguyen, K. A.; Su, S.; Windus, T. L.; Dupuis, M.; Montgomery, J. A., Jr. General atomic and molecular electronic structure system. *J. Comput. Chem.* **1993**, *14*, 1347−1363.
(42) Lane, J. R.; Contreras-García, J.; Piquemal, J.-P.; Miller, B. J.; Kjaergaard, H. G. Are bond critical points really critical for hydrogen bonding? *J. Chem. Theory Comput.* **2013**, *9*, 3263−3266.
(43) Foroutan-Nejad, C.; Shahbazian, S.; Marek, R. Toward a consistent interpretation of the QTAIM: tortuous link between chemical bonds, interactions, and bond/line paths. *Chem. Eur. J.* **2014**, *20*, 10140−10152.
(44) Shishkina, S. V.; Baumer, V. N.; Khromileva, O. V.; Kucherenko, L. I.; Mazur, I. A. The formation of thiotriazoline polymorphs: study from the energetic viewpoint. *CrystEngComm* **2017**, *19*, 2394−2401.
(45) Vaksler, Ye.; Idrissi, A.; Urzhuntseva, V. V.; Shishkina, S. V. Quantum chemical modeling of mechanical properties of aspirin polymorphic modifications. *Cryst. Growth Des.* **2021**, *21*, 2176−2186.
(46) Vaksler, Ye.; Idrissi, A.; Shishkina, S. V. High-pressure influence on piracetam crystals: studying by quantum chemical methods. *Cryst. Growth Des.* **2021**, *21*, 5697−5711.
(47) Shishkina, S. V.; Vaksler, Ye. A.; Konovalova, I. S.; Dyakonenko, V. V.; Varchenko, V. V. Quantum chemical study on mefenamic acid polymorphic forms. *ACS Omega* **2022**, *7*, 17544−17554.
(48) Dolomanov, O. V.; Bourhis, L. J.; Gildea, R. J.; Howard, J. A. K.; Puschmann, H. OLEX2: A complete structure solution, refinement and analysis program. *J. Appl. Crystallogr.* **2009**, *42*, 339−341.
(49) Sheldrick, G. M. SHELXT − Integrated space-group and crystal-structure determination. *Acta Crystallogr., Sect. A: Found. Adv.* **2015**, *A71*, 3−8.
(50) Sheldrick, G. M. Crystal structure refinement with SHELXL. *Acta Crystallogr., Sect. C: Struct. Chem.* **2015**, *71*, 3−8.
(51) Spek, A. L. Structure validation in chemical crystallography. *Acta Crystallogr., Sect. D: Biol. Crystallogr.* **2009**, *65*, 148−155.
(52) Dong, C. PowderX: Windows-95-based program for powder X-ray diffraction data processing. *J. Appl. Cryst.* **1999**, *32*, No. 838.
(53) Rodriguez-Carvajal, J.; Roisnel, T. FullProf98 and WinPLOTR new Windows99/NT applications for diffraction, commission for powder diffraction. *Int. Union Crystallogr. NEWSLETTER* **1998**, *20*, 35−36.
(54) Frisch, M. J.; Trucks, G. W.; Schlegel, H. B.; Scuseria, G. E.; Robb, M. A.; Cheeseman, J. R.et al. *Gaussian 09*, revision B.01; Gaussian, Inc.: Wallingford CT, 2010.
(55) Konovalova, I. S.; Shishkina, S. V.; Paponov, B. V.; Shishkin, O. V. Analysis of the crystal structure of two polymorphic modifications of 3,4-diamino-1,2,4-triazole based on the energy of the intermolecular interactions. *CrystEngComm* **2010**, *12*, 909−916.
(56) Shishkin, O. V.; Dyakonenko, V. V.; Maleev, A. V. Supramolecular architecture of crystals of fused hydrocarbons based on topology of intermolecular interactions. *CrystEngComm* **2012**, *14*, 1795−1804.
(57) Macrae, C. F.; Sovago, I.; Cottrell, S. J.; Galek, P. T. A.; McCabe, P.; Pidcock, E.; Platings, M.; Shields, G. P.; Stevens, J. S.; Towler, M.; Wood, P. A. Mercury 4.0: from visualization to analysis, design and prediction. *J. Appl. Crystallogr.* **2020**, *53*, 226−235.
(58) Coppens, P. The use of a polarized hydrogen atom in X-ray structure refinement. *Acta Crystallogr., Sect. B: Struct. Crystallogr. Cryst. Chem.* **1972**, *28*, 1638−1640.
(59) Allen, F. H.; Bruno, I. J. Bond lengths in organic and metal-organic compounds revisited: X−H bond lengths from neutron diffraction data. *Acta Crystallogr., Sect. B: Struct. Sci.* **2010**, *66*, 380−386.
(60) Schmider, H. L.; Becke, A. D. Optimized density functionals from the extended G2 test set. *J. Chem. Phys.* **1998**, *108*, 9624−9631.
(61) Becke, A. D. Density-functional thermochemistry. V. Systematic optimization of exchange-correlation functionals. *J. Chem. Phys.* **1997**, *107*, 8554−8560.
(62) Weigend, F.; Ahlrichs, R. Balanced basis sets of split valence, triple zeta valence and quadruple zeta valence quality for H to Rn: Design and assessment of accuracy. *Phys. Chem. Chem. Phys.* **2005**, *7*, 3297−3305.
(63) Weigend, F. Accurate Coulomb-fitting basis sets for H to Rn. *Phys. Chem. Chem. Phys.* **2006**, *8*, 1057−1065.
(64) Boys, S. F.; Bernardi, F. The calculation of small molecular interactions by the differences of separate total energies. Some procedures with reduced errors. *Mol. Phys.* **1970**, *19*, 553−566.
(65) Shishkin, O. V.; Zubatyuk, R. I.; Maleev, A. V.; Boese, R. Investigation of topology of intermolecular interactions in the benzene−acetylene co-crystal by different theoretical methods. *Struct. Chem.* **2014**, *25*, 1547−1552.
(66) Neese, F. *ORCA 2.8.0*; Universitaet Bonn: Germany, 2010.
(67) Giannozzi, P.; Baroni, S.; Bonini, N.; Calandra, M.; Car, R.; Cavazzoni, C.; Ceresoli, D.; Chiarotti, G. L.; Cococcioni, M.; Dabo, I.; Dal Corso, A.; de Gironcoli, S.; Fabris, S.; Fratesi, G.; Gebauer, R.; Gerstmann, U.; Gougoussis, C.; Kokalj, A.; Lazzeri, M.; Martin-Samos, L.; Marzari, N.; Mauri, F.; Mazzarello, R.; Paolini, S.; Pasquarello, A.; Paulatto, L.; Sbraccia, C.; Scandolo, S.; Sclauzero, G.; Seitsonen, A. P.; Smogunov, A.; Umari, P.; Wentzcovitch, R. M. QUANTUM ESPRESSO: a modular and open-source software protect for quantum simulations of materials. *J. Phys.: Condens. Matter.* **2009**, *21*, No. 395502.

https://doi.org/10.1021/acsomega.3c01231
ACS Omega 2023, 8, 20661−20674